AIAA'93

AIAA-93-3017

Unsteady Fluid and Optical Simulation of Transonic Aero-Windows

Christopher A. Atwood
MCAT Institute
NASA Ames Research Center
Moffett Field, CA 94035-1000

AIAA 24th Fluid Dynamics, Plasmadynamics, and Lasers Conference
July 6-9, 1993/Orlando, Florida

Unsteady Fluid and Optical Simulation of Transonic Aero-Windows

Christopher A. Atwood,*
MCAT Institute, NASA Ames Research Center,
Moffett Field, California 94035-1000

Abstract

The time-varying fluid and optical fields of several cavity configurations have been computed on overset mesh systems using the Reynolds-averaged Navier-Stokes equations and geometric optics. Comparisons between numerical results and Airborne Optical Adjunct (AOA) flight data are made in two-dimensions for a quieted cavity geometry with two lip-blowing rates. In three-dimensions, two proposed aero-window locations for the Stratospheric Observatory For Infrared Astronomy (SOFIA) are discussed. The simulations indicate that convection of large shear layer structures across the aperture cause the blur circle diameter to be three times the diffraction-limited diameter in the near-infrared band.

Nomenclature

c	speed of sound
dB	decibel, $20\log_{10}\frac{<p'>[N/m^2]}{2\times10^{-5}}$
f	frequency
h	enthalpy
I	intensity
k	wave number, $\frac{2\pi}{\lambda}$
K	ratio of convection by freestream speed
L	characteristic length
$\dot{m}$	mass flow rate
M	Mach number
MTF	modulation transfer function
n	index of refraction
OPD	optical path difference
p	instantaneous static pressure
q	velocity magnitude or dynamic pressure
Re	Reynolds number
St	Strouhal number, $\frac{f\theta}{u_1+u_2}$
SR	Strehl ratio, $\frac{I}{I_0}=\exp(-\Phi^2)$
t	time
T	absolute temperature
T_c	characteristic time, $\frac{L}{Ku_\infty}$
u, v, w	Cartesian velocity components
x, y, z	Cartesian physical space or aperture coordinates
Å	angstrom, $10^{-10}\ m$
α	angle of attack
β	Gladstone-Dale constant, $(n-1)_{STP}$
θ	momentum thickness
λ	wavelength
ρ	density
σ	shear layer spreading rate parameter
Φ	phase, $\frac{2\pi\ OPD}{\lambda}$
$\overline{(\ )}$	mean quantity
$<\ >$	root mean square quantity
$(\ )'$	fluctuating quantity, $f=\overline{f}+f'$

Subscripts

STP	standard temperature and pressure
T	total quantity
∞	freestream quantity

Introduction

The study of light propagating through an unsteady fluid field has important applications ranging from laser weaponry to astronomy platforms. Airborne housing of these systems provides mobility, maintenance, and performance advantages which, in combination, can be superior to land or space-based alternatives. However, prediction of the fluid and optical behavior of these airborne systems remains a difficult problem.

This report describes the progress of a computational approach for use in the design of transonic aero-windows. The prediction methodology has been driven by the design of the Stratospheric Observatory For Infrared Astronomy (SOFIA), the successor to the Kuiper Airborne Observatory (KAO), which will offer ten times the resolution of the KAO. Figure 1 depicts the SOFIA, which will have a 2.5 meter Cassegrain telescope mounted in a cavity of a Boeing 747SP. In order to numerically assess the safety and performance of this platform, extensive evaluation of the computational methods by comparison against experiment is

*Research Scientist, MCAT Institute. Member AIAA.

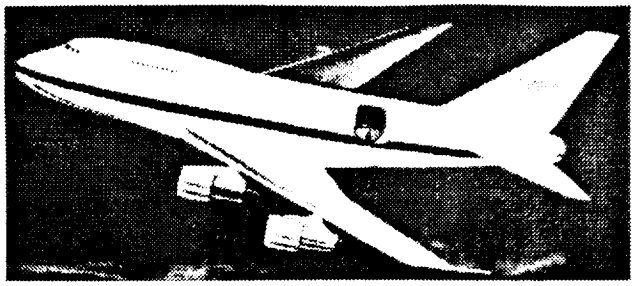

Fig. 1: Artist's concept of the SOFIA configuration

necessary.

Many studies of the effect of a fluid field upon an optical field have been conducted over the past four decades. Many experimental and theoretical approaches to the optical distortion problem have been investigated; only those of which are pertinent to this transonic aero-window problem are summarized here. The experimental efforts can be grouped into two categories: direct measurement methods and techniques based on aerodynamically inferred quantities. Results obtained via the latter method are more prevalent because of practical difficulties in direct measurement techniques.[1] In fact, only aerodynamically inferred distortion levels will used for validation of the present work.

Although early experimental and theoretical efforts assumed incoherent statistical turbulence,[2, 3, 4] recent studies have begun to examine the effect of shear layer structures on electromagnetic field distortion. Using a passive scalar field from a direct numerical simulation, Truman and Lee[5] found an optimum viewing angle normal to the hairpin vortices in the homogeneous sheared fluid region. They also found analysis via non-refracting geometric optics to be equivalent to the parabolized Helmholtz representation of light. Although this class of studies provides excellent insight into the effects of small-scale structure on the electromagnetic field, it is clear that the computational expense of such methods precludes their near-term use for the problems under consideration here.

The study of large scale structures in shear layers has been an active topic of research since they were observed by Brown and Roshko in 1974.[6] Only recently has the effect of these structures on the optical field been studied. In 1990, Chew and Christiansen[7, 8] experimentally observed the effect of shear layer structures on beam propagation. Tsai and Christiansen[9] used an Euler simulation to determine the optical characteristics of a perturbed free shear layer. It was hypothesized that the effect of the vortical structures on the optical field could be modelled by a growing sinusoidal phase plate.

The numerical modelling of the optical effect of a cavity-spanning shear layer was presented by Cassady, Birch, and Terry[10] in 1987. They found their two-dimensional solution to result in poor prediction of optical distortion. Farris and Clark[11, 12] used time-mean quantities and empirical evidence to ascertain the fluctuating density levels required for optical analysis.

The present effort attempts to determine what portion of the optical path distortion can be resolved using cell sizes required to obtain an accurate flowfield solution. Towards this end, computed optical distortion levels are compared to flight or wind tunnel measurements for two- and three-dimensional quieted cavities.

Previous reports[13, 14] have described the method development for two-dimensional free shear layers, a backward-facing step, and a rectangular cavity.[15] Comparison of the computed cavity case with Rossiter's data showed agreement in the dominant resonant peaks to within 5 dB. The computed and experimentally observed pressure loading trends were similar along the cavity walls. In three-dimensions, rectangular and treated quiet cavity solutions were computed and compared to experiment.[16] Sound pressure levels along the cavity bulkheads for both the resonating and quieted geometries were found to be in agreement. However, although the power spectra of the experiment and computation were similar at low frequencies, numerical dissipation caused a rapid decrease in energy content at high frequencies.

Although the optical model has been described previously,[13] this paper documents the extension of the model and provides new validation information. The following sections address the method used to predict the unsteady flows and the resultant optical distortion. Analysis of the aperture fluid and optical fields for AOA and SOFIA configurations are presented. For the two-dimensional AOA geometry, time-varying density fields and optical path lengths are shown. Short and long exposure far-field diffraction patterns are computed for a three-dimensional aft cavity SOFIA concept.

Approach

Solution of the aircraft and cavity flowfields were computed using models for the fluid field, the effect of turbulence, and the optical distortion. A diagonal scheme[17] was used for the solution of the Reynolds-Averaged Navier-Stokes equations, implemented in an overset grid framework.[18] Euler implicit time integration and second-order spatial differencing was used, with viscous impermeable wall conditions specified as no-slip, zero normal pressure gradient, and adiabatic. Information transfer across overset mesh boundaries was implemented using trilinear interpolation of the dependent variable vector, $Q = [\rho, \rho u, \rho v, \rho w, e]^T$. Algebraic turbulence models were used, implemented with a variable F_{max} cutoff for wall-bounded flows and

a shear layer model for the cavity aperture region.[19, 20] The flow solver cost was $13\mu s$/cell/iteration on a single head of the Numerical Aerodynamic Simulator (NAS) Cray Y/MP-832.

Generally, a significant effort in grid generation is required before flow and optical analysis can begin. However, recent advances in algebraic[21] and hyperbolic[22] methods have enabled rapid discretization of complex geometries. Hyperbolic grid generation, which provides spacing and orthogonality control, was used for the wall-bounded regions, while algebraic grids were used in shear flow regions including plumes and wakes. This choice of topology allows simple specification of turbulent regions and also permits the recycling of meshes, useful for configuration changes such as cavity positioning.

The optical computations documented here use a refracting-ray method, reported on earlier, which is limited to studying the effects of the resolved large-scale structures.[23] The method tesselates a structured grid into tetrahedra and uses piecewise mean indices of refraction for each of the tetrahedra. Indices of refraction were computed using $n = 1 + \beta\frac{\rho}{\rho_{STP}}$, where the Gladstone-Dale constant, β, can be found using the Cauchy formula.

Assessment of the optical performance of an aero-window begins by specification of the ray initialization plane. Integration of the optical path length through the aero-window is then performed along the rays at specified time increments in both the streamwise, x, and crossflow, y, aperture directions. The resultant $OPD(t,x,y)$ can be used in a complex aperture function of the form $P = A\, e^{i\Phi(t,x,y)}$. Assuming no loss in transmittance, then the wave amplitude A is unity in the aperture and zero elsewhere, while the phase of the wave is computed from $OPD(t,x,y) = \frac{\lambda\Phi}{2\pi}$. The autocorrelation of the complex aperture function, $P * P$, gives the far field diffraction pattern, computed using a two-dimensional Fourier transform. Time averaging successive short-period diffraction patterns gives a long exposure result. Integration of the intensity of this resultant long or short exposure diffraction pattern gives the area for a specified encircled energy level. From this area the equivalent blur-circle diameter due to the resolved fluid scales can be found. Inclusion of the effects of small-scale turbulence could be incorporated into the computation of long exposure blur circles by multiplication of the above modulation transfer function (MTF) with a turbulence MTF.[3, 24]

Results and Discussion

Aero-optical simulations of the U.S. Army Airborne Optical Adjunct (AOA) and the SOFIA configurations are discussed below. Information pertaining to the computation and analysis of the unsteady flowfields, including grid resolution and turbulence modelling, is given elsewhere.[14, 23]

2-D AOA Cavities

Data available from flight tests of the AOA,[25] shown in Fig. 2, provides valuable validation information for

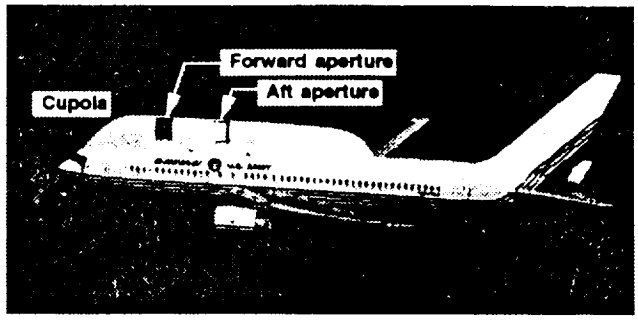

Fig. 2: U.S. Army Airborne Optical Adjunct

the present simulations. These two-dimensional numerical simulations were used to determine if optical quieting methods, particularly aft ramp treatment and lip-blowing, could be accurately simulated. The flow about the geometry, depicted in Fig. 3, was computed in conjunction with two lip-blowing rates for the forward aperture only. The 100% lip-blowing rate case corresponded to a $\dot{m} = 0.42(\rho u)_\infty$. For the discussion below, computed high and low lip-blowing rates refer to 100% and 1% of this mass flow rate.

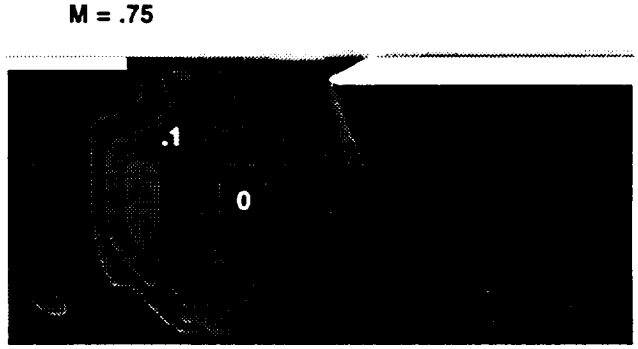

Fig. 3: AOA case: instantaneous Mach contours

Computed and flight mean Mach number profiles are compared in Fig. 4 for two lip-blowing rates, with instantaneous Mach number contours shown above each set of profiles. The quantity ϕ indicates the angle from the cupola crest at which the data was measured. Overall, the Mach number contours, which were averaged over 2000 time steps, show agreement in the maximum vorticity as a function of x-station. However, differences exist between experimental and computational results at the low-speed edge of the shear layer,

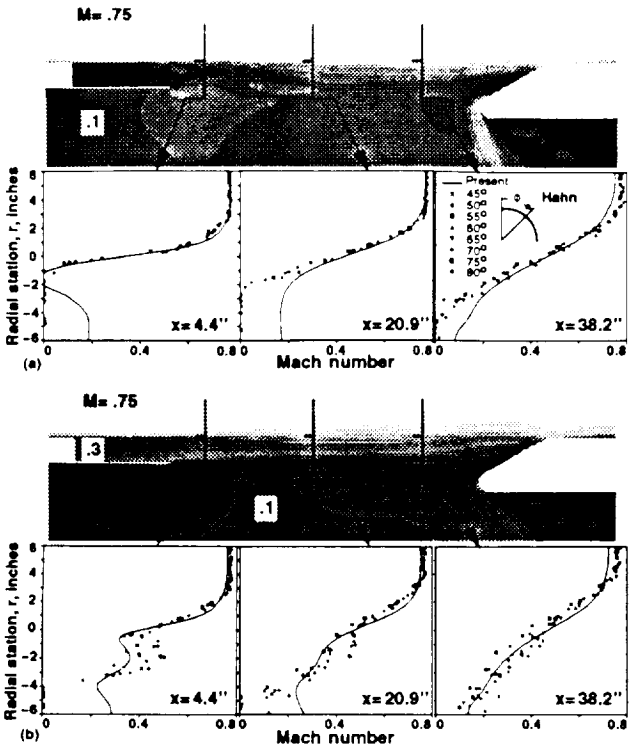

Fig. 4: AOA case: instantaneous Mach number contours and mean profiles at (a) low and (b) high lip-blowing rate

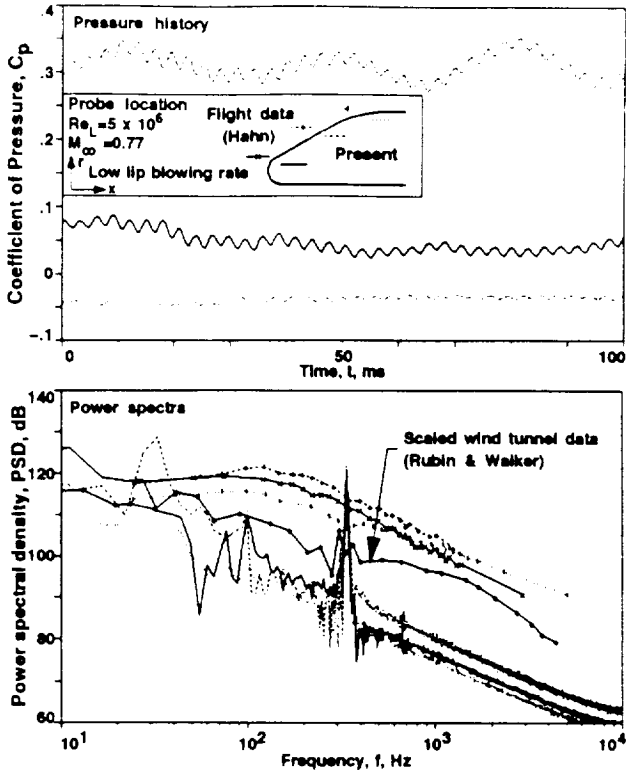

Fig. 5: AOA case: power spectra, low lip-blowing rate

which may be due to blockage in the cavity of the aircraft that was not computationally represented. The discrepancy at the upper aft portion of the shear layer appears to be due to blockage in the computational model.

Comparisons of pressure spectra at the aft ramp for the low lip-blowing rate are shown in Fig. 5. The computed spectra can be seen to be quantitatively and even qualitatively different from flight data. The computed result lies more than 15 dB below the data, and a peak in the low lip-blowing rate spectra is clearly computed, but is not seen in the flight data. The high lip-blowing rate spectra were similar to that shown in Fig. 5, albeit without the spectral peak at 340 Hz.[23]

It has been noted from experimental evidence[26] that the frequency of large structures in shear layers is independent of axial station and occurs at Strouhal number of $St = \frac{f\theta}{u_1+u_2} = 0.024 \pm 0.003$, where θ is the local shear layer momentum thickness and f denotes frequency. This phenomena is corroborated by the reduction of other researchers' data,[6, 7, 9, 27, 28] whose results range from about $St = 0.02$ to 0.03 for incompressible shear layers.

Momentum thickness can be estimated using Görtler's solution, giving $\theta = 0.036\frac{1-r}{1+r}x$ for $\sigma_0 = 11.0$, which compares favorably to the empirically determined correlation[29] of $\theta = 0.034\frac{1-r}{1+r}x$. Using this relationship along with a compressibility correction,[30] the computed peak in the AOA solution at 340 Hz corresponds to a Strouhal number of 0.032. For comparison, peaks were found in SOFIA experiments and computations at approximately $St = 0.028$.

Based upon these experimental observations, it is hypothesized that large scale shear layer structures are being resolved. However, the lack of empirical support from the flight data pressure power spectra is at odds with this conclusion. The comparison is further clouded by the reasonable comparison in $< \rho' >$ for the low lip-blowing rate shown in Fig. 6, and the presence of the organized structures shown in Fig. 7.

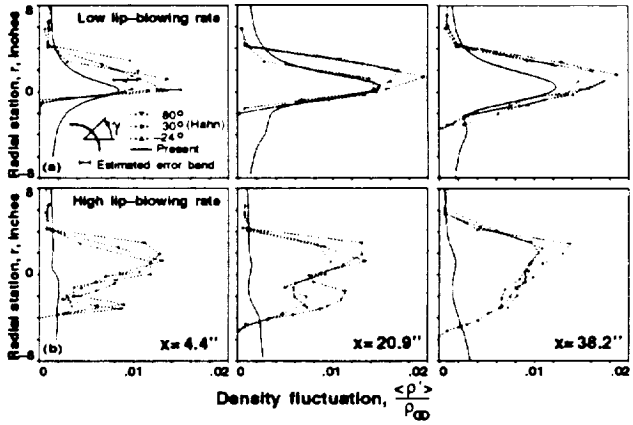

Fig. 6: AOA case: $\frac{<\rho'>}{\rho_\infty}$ profiles with (a) low and (b) high lip-blowing

Three-dimensional effects are a possible explanation for the discrepancy between computation and flight. Rockwell[31] noted that for sufficiently large Reynolds numbers three-dimensionality reduces coherence in the shear layer. This implies that an error in the assumption of planar flow for the small flow oscillations considered in these quieted cavity configurations. The evolution of streamwise-oriented vorticity interacting with the primary vortices would act to spread peaks in the reattachment ramp pressure spectra. As a final note, Fig. 5 also depicts data, the ordinate scaled by $(q_\infty)_{flight}/(q_\infty)_{tunnel}$ and the abcissa by $(c_\infty/L)_{flight}/(c_\infty/L)_{tunnel}$, obtained from an AOA wind tunnel test.[32] The wind tunnel data shows that a small peak exists where expected according to the above analysis.

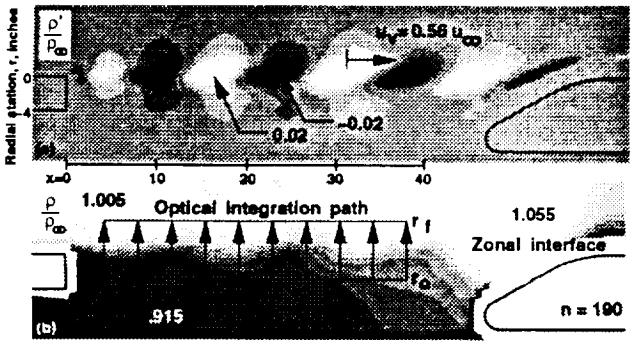

Fig. 7: AOA case, low lip-blowing rate: instantaneous contours of (a) $\frac{\rho'}{\rho_\infty}$ and (b) $\frac{\rho}{\rho_\infty}$ with schematic of optical model

Using the computed unsteady density field, aero-optical effects can be determined. Figure 6 compares the computed and experimental profiles of the root mean square of the density fluctuations. Levels of $< \rho' >$ were computed over a time segment of about 90 ms in increments of 0.44 ms. Using the elapsed time for a particle to convect across the aperture at the mean shear layer speed as a characteristic time, then the optical computation was taken for about nine T_c. In Fig. 6, γ is the rake angle from horizontal, with the axis of rotation offset from the cupola centerline. Determination of the systematic error band on the experimental result is discussed below. The low lip-blowing rate result underpredicts the magnitude of the peak in $\frac{<\rho'>}{\rho_\infty}$, however the peak location is in fair agreement. The computed results for the high lip-blowing rate compare poorly to experiment, possibly due to inadequate grid resolution and/or the increased flow complexity of the merging shear layers. This type of active control is presently not a design option for the SOFIA, therefore further effort toward improvement of the high lip-blowing case was not warranted.

Further investigation of the low-blowing rate case revealed the presence of large convecting structures associated with the shear layer. Figure 7 shows a contour plot of $\frac{\rho'}{\rho_\infty}$, depicting the growth and propagation of these shear layer structures. Also depicted in Fig. 7 is a schematic of the optical model, with the initial and final stations of the optical path integration given by r_0 and r_f. The large structures, associated with a $0.03u_\infty$ vertical velocity component, are the primary contributors of the computed density fluctuations of the shear layer. The speed of the waves, as determined from Fig. 8, is $0.56u_\infty$, below the value of $0.66u_\infty$ inferred by Rossiter[15] for rectangular cutouts, yet above the $0.51u_\infty$ determined analytically by Roscoe and Hankey.[33]

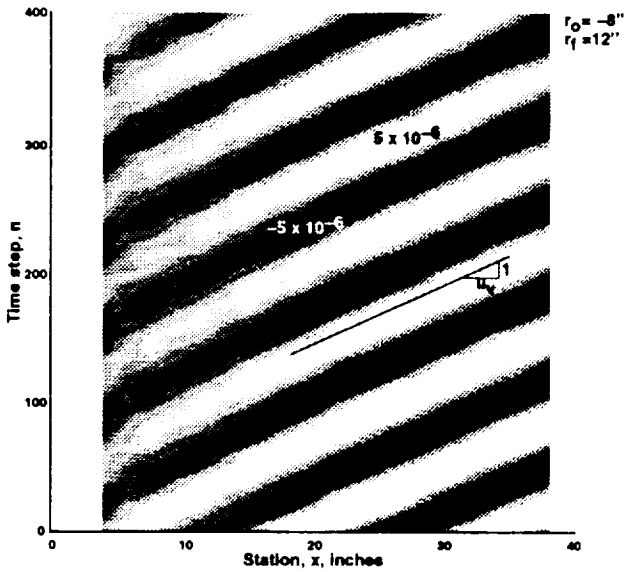

Fig. 8: AOA case: contours of $OPD'(x,t)$[$in.$] along aperture, low lip-blowing rate

In 1990, Chew and Christiansen[8] and Tsai and Christiansen[9] deduced that a free shear layer model of a sinusoidal phase delay growing in x would produce results similar to those observed in both computation and experiment. Figure 8 displays behavior of a similar nature for the aero-window problem of concern here.

Comparisons of integrated aero-optical quantities, shown in Fig. 9, reveal slight overprediction for the low lip-blowing case and, given the $< \rho' >$ profiles, expected underprediction for the high lip-blowing rate case. Also shown in Fig. 9 are the $< OPD' >$ for two additional integration paths, shown to demonstrate that most of the optical distortion is caused by the shear layer.

The result for the integration path which extends from $r_0 = -8''$ to $r_f = 12''$ displays an increment in $< OPD' >$ of about $(7 \times 10^{-7})''$ from the $7''$ path length case which passes through the shear-layer alone. The path initialized above the shear layer, from $r_0 = 4''$ to $r_f = 12''$, shows a small $< OPD' >$ indicating

that $< \rho' >$ above the shear layer is small. Finally, the time mean optical path difference, $\overline{OPD}$, can be seen to contribute curvature to the wavefronts as the light propagates through the shear layer. The optical clarity of the shear layer was determined using a $\beta = 2.584 \times 10^{-4}$, matching the value which was used to reduce the experimental data.

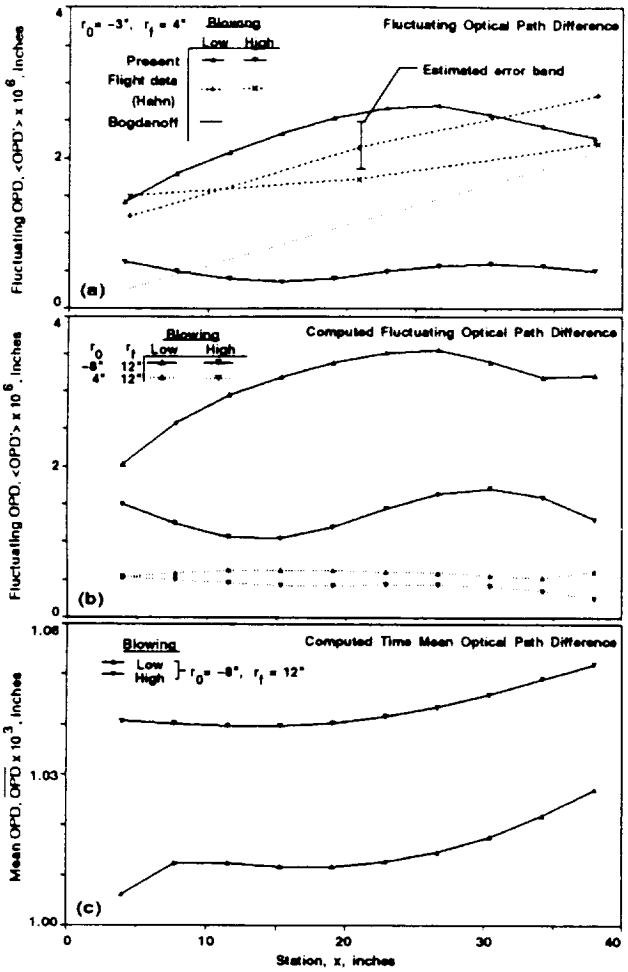

Fig. 9: AOA case: streamwise variation of optical path difference quantities

The analytic result for the $< OPD' >$, which goes like x, is found from[34]

$$(\overline{\Phi})^2 = \left(\frac{2\pi < OPD' >}{\lambda}\right)^2 = 2k^2 \frac{b^3}{a} L_{50n,m}^3 \int_0^{L_{50n,m}} \left(\frac{\partial n}{\partial y}\right)^2 dy$$

Derivation of the model, which utilizes time-mean quantities to determine $< OPD' >$, is given by Bogdanoff.[34] This analytic result assumes an index-matched shear layer with a sinusoidal n profile, $n(y) = \frac{n_1 - n_{max}}{2} \sin\left(\frac{2\pi y}{2L_{50n,m}}\right)$. The constants, $\frac{b^3}{a} = 0.0091$ and $L_{50n,m} \approx 1.31\delta_\omega = 1.31(0.18x[m])$, are empirical relations. The virtual origin of the shear layer is placed at $x = 0''$ to obtain this analytic result. As shown in Fig. 9, the analytic gradient in $< OPD' >$ is in good agreement with flight data.

Reduction of Experimental Data

The reduction of the data obtained from experiment[35] is noted here to delineate the approximations used and estimate systematic error bounds in the optical path distortion levels. Values of ρ' are computed from assumptions of quasi-steady flow:

$$h_T = c_p T \left(1 + \frac{\gamma - 1}{2} M^2\right)$$

Differentiation with respect to t gives

$$RT_T' = \frac{\rho p' - p\rho'}{\rho^2} + uu' \frac{\gamma - 1}{\gamma}$$

Using $(\rho u)' = \rho u' + \rho' u$ then

$$\frac{T_T'}{T} = \frac{p'}{p} + (\gamma - 1)M^2 \frac{(\rho u)'}{\rho u} - \left[(\gamma - 1)M^2 + 1\right] \frac{\rho'}{\rho}$$

The experimental observations against which the computed results are compared assume simultaneously small fluctuations in pressure and total temperature,[36, 37] resulting in

$$\frac{\rho'}{\overline{\rho}} = \left(\frac{1}{(\gamma - 1)\overline{M}^2} + 1\right)^{-1} \frac{(\rho u)'}{\overline{\rho u}} \qquad (1)$$

Mean Mach number and density profiles are determined from isentropic relations, while $\frac{(\rho u)'}{\overline{\rho u}}$ is proportional to the voltage fluctuation, $\frac{E'}{E}$, obtained from hot film probes. The optical path disturbance is then found from[1]

$$(OPD')^2 = 2\left(\frac{\beta}{\rho_{STP}}\right)^2 \int_0^L < \rho' >^2 l_r dr \qquad (2)$$

where $\frac{l_r}{L}$ is the turbulent eddy size relative to the shear layer width, determined from cross correlation data to be typically about 15%.

The few available independent measurements[37, 38] indicate that pressure fluctuations of about 2% of freestream static pressure occur in the shear layer spanning the aperture of a quieted cavity geometry. In fact, Hahn[25] reported pressure fluctuations of 8% from shear layer rake measurements, however these include the dynamic pressure component normal to the orifice as well. Pressure fluctuation levels can also be inferred from sound pressure levels in the cavity, observed to be at least 130 dB for the AOA case. Shear layer total temperature fluctuations of about 1% have also been reported for this Mach regime.[38] The present low lip-blowing computation found a $< p' > \approx 1\%$ and

a $< T_T' > \approx 0.8\%$ in the shear layer. The assumption of $< T_T' >$, $< p' > \approx 0$ in a shear layer is therefore questionable, and is used to estimate systematic experimental error bounds.

The determination of the error in $< \rho' >$ due to background noise levels begins by assuming the passage of a compression wave parallel to the static pressure port in the wake rake. Normal reflection of the wave would impart a larger deviation from $< \rho' >$ as computed by Eq. 1. Utilizing Görtler's free shear layer solution to provide $\overline{u(r)}$, assuming a cavity temperature recovery factor of unity, and holding mean static pressure constant through the layer, then $\overline{\rho(r)}$ is defined. The sensitivities of $\frac{\rho'}{\overline{\rho}}$ to $\frac{p'}{\overline{p}}$ and $\frac{T_T'}{\overline{T_T}}$ are $\pm\frac{1}{(\gamma-1)M^2+1}$ and $\mp\frac{(1+(\gamma-1)M^2/2)}{(\gamma-1)M^2+1}$, respectively. Using a compression or rarefaction wave of strength $< p' >$ through the shear layer, then local values of ρ' due to wave passage are defined. This value of ρ' provides the error bound about the value obtained from Eq. 1, which assumes negligible $< p' >$ and $< T_T' >$. Taking shear layer pressure fluctuation levels corresponding to 135 dB and a velocity ratio $r = 0.1$, then the systematic error in the density fluctuations is 0.13% at the shear layer center. Figure 6 shows the resultant systematic error bars in $< \rho' >$.

From Eq. 2 the value of $< \rho' >$ is linearly proportional to $< OPD' >$. The error in $< OPD' >$ can be found by using a conservative within-system error of 0.05% in $\frac{<\rho'>}{\rho_\infty}$ gleaned from Fig. 6, plus the systematic error from the above analysis. The resultant error bar is plotted in Fig. 9.

Forward Cavity SOFIA

Wind tunnel tests, completed in 1990, allowed validation of cavity acoustic response and optical characteristics. The cavity environment results are summarized in Fig. 10 for both resonant and quieted configurations.[13] Aerodynamic measurements in the shear layer were used to infer optical quantities for the quieted cavity, configuration 100.

Following computation of the unsteady flow, the optics code was applied to the computed density field obtained for configuration 100 from $t = 0$ to 7.8 ms. Ten rays were propagated through 110 instantaneous density fields in time intervals of $\Delta t = 70.6\mu s$. The optical measurement was taken for about five T_c, again using the elapsed time for a shear layer structure to convect across the aperture as the characteristic time. The forward cavity SOFIA results presented here are for a computational plane at approximately the cross flow center of the aperture, which will provide only a streamwise variation in optical properties. The numerical results are presented compared to previous analysis[34] and experiment[16] in which shear layer aerodynamic measurements were used to infer distortion.

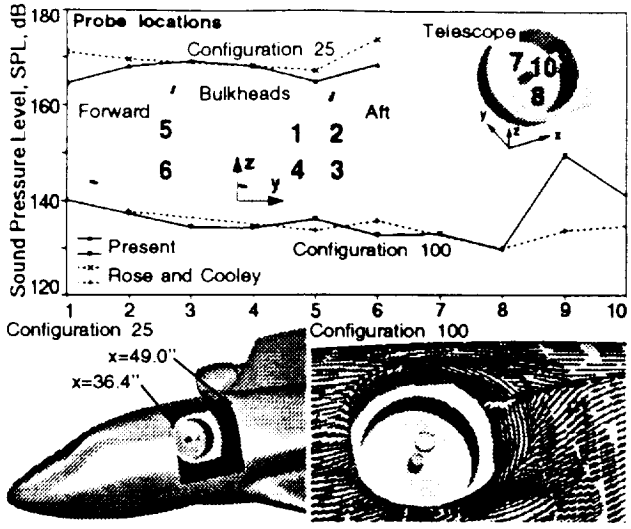

Fig. 10: Forward cavity SOFIA cases: Comparison of sound pressure levels

Comparison of experimental and numerical density fluctuations are shown in Fig. 11, where $< \rho' >$ can be seen to be severely underpredicted. Although peaks in the density fluctuations were computed, the highly-ordered shear layer structures similar to those found in the AOA study were not observed. Differences may be attributable to grid coarseness or within-system measurements errors.

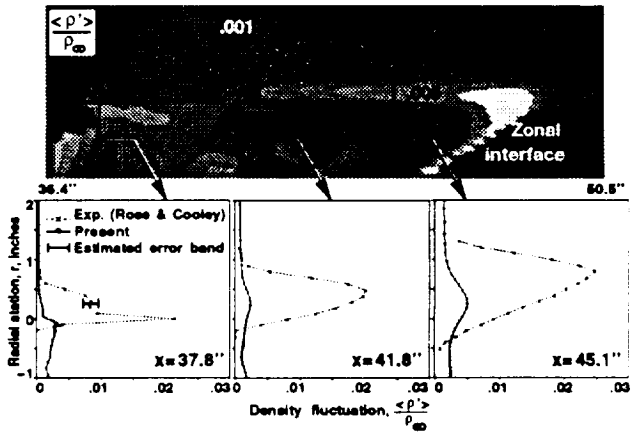

Fig. 11: Configuration 100: density fluctuation at cross-flow center of aperture

The optical wavefront distortion through the configuration 100 aero-window is summarized in Fig. 12. Figure 12a shows that the distortion model applied through the shear layer alone underpredicts the data determined analytically and experimentally. However, the computed trend is generally consistent with the data. At the streamwise center of the aperture, the aerodynamically inferred $< OPD' >$ at two additional

spanwise locations are shown. These points provide an estimate of the crossflow variation in experimental distortion levels.

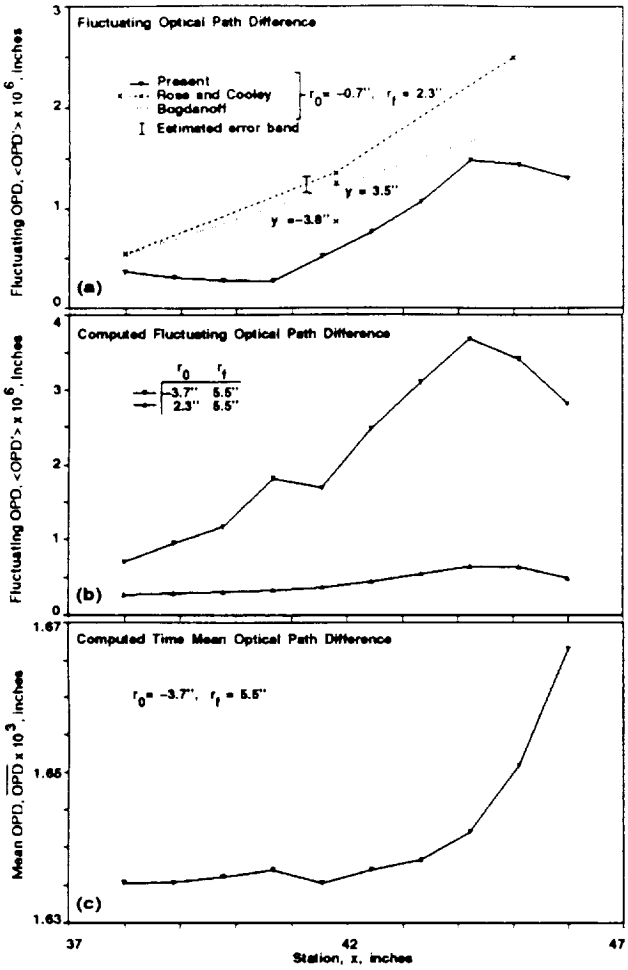

Fig. 12: Configuration 100: comparison of wavefront distortion

Figure 12b depicts computed $< OPD' >$ for ray propagation originating below the secondary mirror, $r_0 = -3.7''$, and above the shear layer, $r_0 = 2.3''$. Comparison of the computed results show an increment in $< OPD' >$ below the secondary mirror. This distortion increment appears to be caused by a jet of re-entrant fluid originating from the shear layer impinging on the aft ramp. Finally, Fig. 12c shows that curvature is imparted to the mean optical field. The dip in the fluctuating and mean OPD levels at $x = 42''$ is caused by the presence of the secondary mirror, in which the index of refraction, n, was fixed at unity.

Aft Cavity SOFIA

Forward placement of the telescope in a favorable pressure gradient region has an advantage in terms of an optically thin boundary layer. However, the fuselage moldline and structural complexities forward of the wing present considerable manufacturing difficulties. An alternative site for the telescope aft of the wing reduces the modification costs and permits the use of a larger usable cavity volume. However, an aft cavity site has potential problems of scattered light emitted from engines and plumes, an optically thick boundary-layer, unknown cavity response, and possibly poor empennage flow behavior at off-design conditions.

Figure 13 depicts the simplified geometry used to address some of these concerns; horizontal and vertical stabilizer geometry was unavailable for this simulation. Details of this flight condition simulation are available elsewhere.[14]

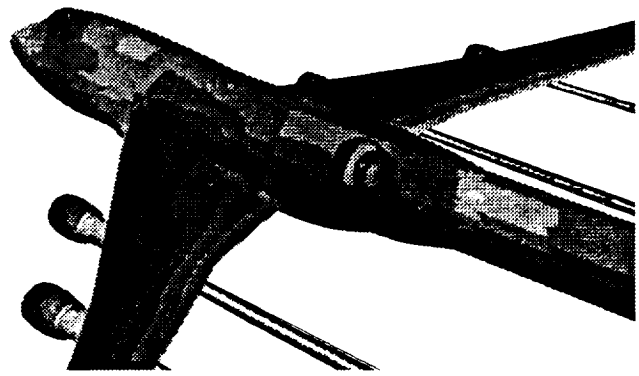

Fig. 13: Aft SOFIA case: Surface C_p and plume temperature contours

The acoustic response of the aft cavity is compared to scaled data from the forward cavity experiment in Fig. 14. The computed result is taken from a location

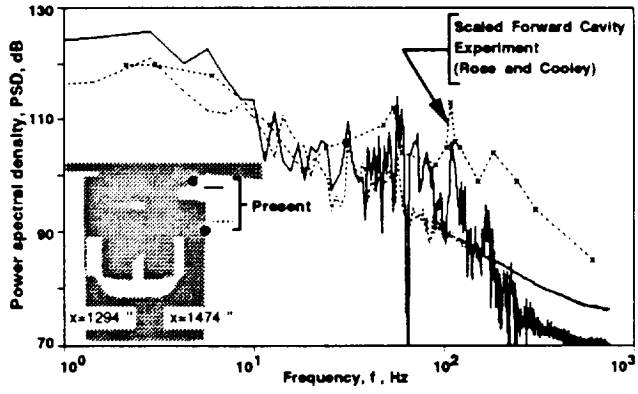

Fig. 14: Aft SOFIA case: Power spectra comparison

on the aft ramp, while the experiment is from a location within the cavity. The agreement of spectra is reasonable to about 100 Hz, above which grid coarseness dissipates energy rapidly.[14] Figure 14 shows peaks at 60 and 110 Hz, the latter corresponding to a Strouhal number of 0.028.

During the aft cavity SOFIA computation the entire aperture density field was saved in increments of

0.68 ms, every five flow solution steps. Using this density field, propagation of a plane wave through the aperture revealed variations in the wavefront distortion, as shown in Fig. 15. These ordered variations in OPD, indicative of shear layer structures in the aperture, impact the aft ramp at a frequency of 110 Hz, giving a $St = 0.028$. Figure 15 shows maximum distortions of about one wavelength, $\pm\lambda_D$, with a resultant maximum $< OPD' >$ of approximately $0.7\lambda_D$. Computation of the $OPD(t, x, y)$ was performed for a 64 x 64 array of rays normal to the aperture and initialized just above the secondary mirror. The optical integration was performed over 8 T_c.

Fig. 15: Aft SOFIA case: Sample wavefront distortion history

Using these phase distortion levels, far field diffraction patterns were then computed. Figure 16 depicts the diffraction-limited Airy pattern for reference, and both instantaneous and time-averaged exposures. The instantaneous exposure pattern shows some evidence of speckle, with a large reduction in central peak intensity. This spreading of energy is manifested in the computed Strehl ratio of 0.34.

Finally, Fig. 17 shows that the large scale structures in the shear layer cause the equivalent 80% blur circle to be three times the diameter of the diffraction-limited case. However, as can be seen in Fig. 16, the blurring in the streamwise direction is worse than in the crossflow direction. Note that the because the small scale fluid motion is modelled when using the Reynolds-averaged Navier-Stokes equations, the computed blur circle is much smaller than actually observed.[39]

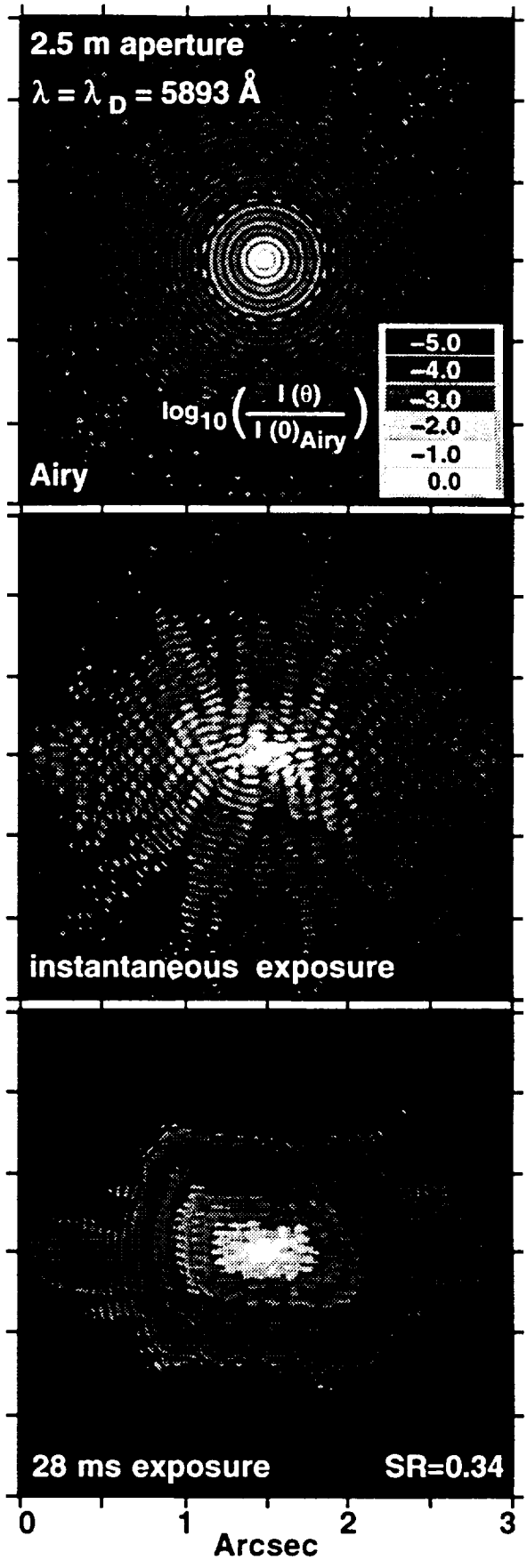

Fig. 16: Aft SOFIA case: Far field diffraction patterns

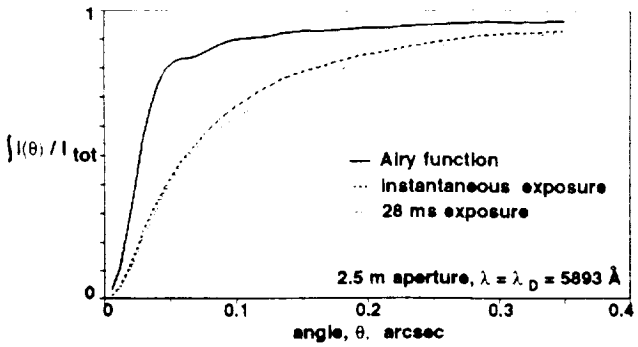

Fig. 17: Aft SOFIA case: Normalized integrated intensity distributions

Conclusions

Computations of quieted cavity configurations have shown convection of large scale flow structures across the aperture. The shedding frequency of these structures compare reasonably well with experimentally determined shear layer Strouhal numbers. The computed results indicate that three-dimensional effects on the shear layer spanning a quieted cavity can be significant. The differences in two- and three-dimensional results are manifested in the spectra of the pressure loads and in the magnitude of the optical wavefront distortion. Since the primary contributors to the computed OPD' were the large scale structures, computations of the Strehl ratio were found to be reasonable. However, because the small scale fluid motion is modelled, the blur circle diameter is significantly underpredicted.

Further improvements to the prediction of optical performance may be found from investigation of shear regions with direct Navier-Stokes methods[5] or use of a turbulence MTF.[24] Finally, although low Reynolds and Mach number number experiments show large structure formation, direct OPD measurements at realistic conditions would be useful for validation of numerical aero-optical studies of this type.

Acknowledgements

This investigation was supported by grant NCC-2-677. Special thanks is due to Dr. E.W. Dunham for insightful comments regarding seeing and optical diffraction.

References

[1] Gilbert, K., "KC-135 Aero-Optical Turbulent Boundary Layer/Shear Layer Measurements," *Aero-Optical Phenomena*, Vol. 80, Progress in Astronautics and Aeronautics, AIAA, New York, 1982.

[2] Stine, H.A. and Winovich, W., "Light Diffusion Through High-Speed Turbulent Boundary Layers,"NACA RM-A56B21, 1956.

[3] Sutton, G.W., "Effect of Turbulent Fluctuations in an Optically Active Fluid Medium," *AIAA J.*, Vol. 7, Sep. 1969, pp. 1737-1743.

[4] Sutton, G.W., "Aero-optical Foundation and Applications," *AIAA J.*, Vol. 23, Oct. 1985, pp. 1525-1537.

[5] Truman, C.R. and Lee, M.J., "Effects of organized turbulence structures on the phase distortion in a coherent optical beam propagating through a turbulent shear flow," *Phys. Fluids A*, Vol. 2, May 1990, pp. 851-857.

[6] Brown, G.L. and Roshko, A., "On density effects and large structure in turbulent mixing layers," *J. Fluid Mech.*, Vol. 64, Part 4, 1974, pp. 775-816.

[7] Chew, L. and Christiansen, W., "Coherent Structure Effects on the Optical Performance of Plane Shear Layers," *AIAA J.*, Vol. 29, Jan. 1991, pp. 76-80.

[8] Chew, L. and Christiansen, W., "Experimental Investigation of Free Shear Layer Optics," Paper No. AIAA-91-1722, June 1991.

[9] Tsai, Y.P. and Christiansen, W.H., "Two-Dimensional Numerical Simulation of Shear-Layer Optics," *AIAA J.*, Vol. 28, Dec. 1990, pp. 2092-2097.

[10] Cassady, P., Birch, S.F., and Terry, P.J., "Aero-Optical Analysis of Compressible Flow Over An Open Cavity," Paper No. AIAA-87-1399, June 1987.

[11] Clark, R.L. and Farris, R.C., "A Numerical Method to Predict Aero-Optical Performance in Hypersonic Flight," Paper No. AIAA-87-1396, June 1987.

[12] Farris, R.C. and Clark, R.L., "An Integrated Navier-Stokes and Wave Optics Numerical Simulation Technique for Predicting the Aero-Optical Performance about Subsonic Surveillance Aircraft," Paper No. AIAA-88-0753, Jan. 1988.

[13] Atwood, C.A., and Van Dalsem, W.R., "Flowfield Simulation about the SOFIA Airborne Observatory," Paper No. AIAA-92-0656, Jan. 1992. *AIAA J. of Aircraft*, to appear.

[14] Atwood, C.A., "Selected Computations of Transonic Cavity Flows," Forum on Computational Aero- and Hydro-Acoustics, 1993 ASME Fluids Engineering Conference, Washington D.C., June 1993.

[15] Rossiter, J. E., "Wind-Tunnel Experiments on the Flow Over Rectangular Cavities at Subsonic and Transonic Speeds," Royal Aircraft Establishment Reports and Memoranda No. 3438, Oct. 1964.

[16] Rose, W.C. and Cooley, J.M., "SOFIA Wind Tunnel Data Analysis and Implications for the Full-Scale Aircraft," Rose Eng. and Research, Inc., Dec. 1990.

[17] Pulliam, T.H. and Chaussee, D.S., "A Diagonal Form of an Implicit Approximate-Factorization Algorithm," *J. Comp. Phys.*, Vol. 39, Feb. 1981, pp. 347-363.

[18] Benek, J.A., Buning, P.G., and Steger, J.L., "A 3-D Chimera Grid Embedding Technique," Paper No. AIAA-85-1523, July 1985.

[19] Baldwin, B.S. and Lomax, H., "Thin-Layer Approximation and Algebraic Model for Separated Turbulent Flows," Paper No. AIAA-78-257, Jan. 1978.

[20] Buning, P.G. and Chan, W.M., "OVERFLOW/F3D User's Manual, Version 1.5," NASA/ARC, Nov. 1990.

[21] Steinbrenner, J.P., Chawner, J.R., and Fouts, C.L., "A Structured Approach to Interactive Multiple Block Grid Generation," AGARD FDP Specialists Mtg. on Mesh Generation for Complex Three-Dimensional Configurations, Loen, Norway, May 1989.

[22] Chan, W.M. and Steger, J.L., "Enhancements of a Three-Dimensional Hyperbolic Grid Generation Scheme," *App. Math. and Comp.*, Vol. 51, pp. 181-205.

[23] Atwood, C.A., "Navier-Stokes Simulations of Unsteady Transonic Flow Phenomena," NASA TM-103962, Aug. 1992.

[24] Richardson, M.B., and Clark, R.L.,"Prediction of image degradation through a turbulent medium," *Flow Visualization and Aero-Optics in Simulated Environments*, Vol. 788, SPIE, May 1987, pp. 2-9.

[25] Hahn, M.M., "Flight Test Verification of the Aerodynamic Characteristics of the 767-AOA Open Viewports," Boeing Commercial Airplane Company, Doc. D041T207TN, Fall 1987.

[26] Hussain, A.K.M.F. and Zaman, K.B.M.Q., "An experimental study of organized motions in the turbulent plane mixing layer," *J. Fluid Mech.*, Vol. 159, 1985, pp. 85-104.

[27] Oster, D. and Wygnanski, I., "The forced mixing layer between parallel streams," *J. Fluid Mech.*, Vol. 123, 1982, pp. 91-130.

[28] Winant, C.D. and Browand, F.K., "Vortex pairing: the mechanism of turbulent mixing-layer growth at moderate Reynolds number," *J. Fluid Mech.*, Vol. 63, 1974, pp. 237-255.

[29] Roberts, F.A. and Roshko, A., "Effects of Periodic Forcing on Mixing in Turbulent Shear Layers and Wakes," Paper No. AIAA-85-0570, Mar. 1985.

[30] Bogdanoff, D.W., "Compressibility Effects in Turbulent Shear Layers," *AIAA J.*, Vol. 21, June 1983, pp. 926-927.

[31] Rockwell, D., "Oscillations of Impinging Shear Layers," Paper No. AIAA-82-0047, Jan. 1982.

[32] Rubin, D.V. and Walker, B.J., "AOA Aero-Optical Wind Tunnel Test Final Analysis Report," Technical Report RD-SS-86-8, U.S. Army Missile Command, Feb. 1986.

[33] Roscoe, D.F. and Hankey, W.L., "The Stability of a Compressible Free Shear Layer," AFWAL-TR-80-3016, Oct. 1979.

[34] Bogdanoff, D.W., "The Optical Quality of Shear Layers: Prediction and Improvement Thereof," *AIAA J.*, Vol. 22, Jan. 1984, pp. 58-64.

[35] Rose, W.C. and Johnson, D.A., "Unsteady Density and Velocity Measurements in the $6' \times 6'$ Wind Tunnel," Proceedings of the Aero-Optics Symposium on Electromagnetic Wave Propagation from Aircraft, NASA CP-2121, Aug. 1979, pp. 153-181.

[36] Cebeci, T. and Smith, A.M.O., *Analysis of Turbulent Boundary Layers*, Academic Press, New York, 1974.

[37] Johnson, D.A. and Rose, W.C., "Turbulence Measurement in a Transonic Boundary Layer and Free-Shear Flow Using Laser Velocimetry and Hot-Wire Anemometry Techniques," Paper No. AIAA-76-399, July 1976.

[38] Raman, K.R., "Pressure and Temperature Fields Associated with Aero-Optics Tests," Proceedings of the Aero-Optics Symposium on Electromagnetic Wave Propagation from Aircraft, NASA CP-2121, Aug. 1979, pp. 91-121.

[39] Dunham, E.W., Private communication, NASA/ARC.

APPENDIX E